(Preprint) AAS XX-XXX

ADVANCING ASTEROID SPACECRAFT GNC TECHNOLOGY USING STUDENT BUILT CUBESAT CENTRIFUGE LABORATORIES

Ravi teja Nallapu[*], Stephen Schwartz[†], Erik Asphaug[‡] and Jekan Thangavelautham[§]

Asteroid science, technology, and exploration is an important and exciting research and education theme at the University of Arizona (UA) that encompasses the College of Science and College of Engineering. Here we outline UA's future efforts in developing new facilities and technologies to advance asteroid exploration with major implications to GNC. UA is planning to develop a research and education center called ASTEROID (Asteroid Science, Technology and Exploration Research Organized by Inclusive eDucation (ASTEROID) funded by NASA. This proposed program envisions project-centric, hands-on education that would place UA students and transfer students from the nearby Pima Community College and the University of Puerto Rico, Humacao in cutting-edge research labs at the UA and in direct collaboration with NASA JPL. UA, Pima, and Univ. of Puerto Rico students would be tasked with developing an exciting series of CubeSat missions. First among these is the development of the AOSAT+ CubeSat mission concept which is presented in this paper. The mission consists of a 12U CubeSat that will operate as a centrifuge laboratory in low Earth orbit. The CubeSat will carry crushed meteorite, along with a suite of science instruments. The spacecraft will rotate at 0.1 to 1.1 RPM to simulate the milli-gravity environment of a desired small body. A major challenge with operating a centrifuge spacecraft is that it contains shifting masses, which result in perturbation torques on the spacecraft. This requires a robust attitude controller to spin the spacecraft at its target rotation speed. This work presents the development of a sliding mode attitude control law that enables the operation of the AOSAT+ Centrifuge mode.

INTRODUCTION

The surfaces of asteroids are challenging to explore due to their low gravity. For this reason, active missions to asteroids such as OSIRIS-Rex [1] and Hayabusa-2 [2] rely on short duration touch and go operations which mitigates the risk. There are a large number of asteroids known (about 2 million asteroids in the main belt), which exhibit a diverse set of physical characteristics, composition, and origin [3]. Despite these challenges, understanding asteroid surfaces can yield high-value science return [4].

[**] PhD Candidate, Space and Terrestrial Robotic Exploration (SpaceTREx) Laboratory, Univ. of Arizona, 85721.
[††] Postdoctoral Fellow, Lunar and Planetary Laboratory, Univ. of Arizona, 85721.
[‡] Professor, Lunar and Planetary Laboratory, Univ. of Arizona, 85721.
[§] Assistant Professor, Space and Terrestrial Robotic Exploration (SpaceTREx) Laboratory, Univ. of Arizona, 85721.

To address these challenges, we propose a series of successor missions to AOSAT 1. This include a large platform mission concept called AOSAT+ [5], which will simulate the surface of a desired asteroid inside a 12U CubeSat spacecraft in a Low Earth Orbit (LEO). The surface generation is achieved by spinning the spacecraft about one of its fixed axes on its orbit. The concept of operations of the AOSAT+ mission is presented in Figure 1. The internal layout of the spacecraft is shown in Figure 2. As seen here, after launch and deployment, the spacecraft will enter into a commissioning mode. In this mode, the spacecraft performs a detumble maneuver to nullify any angular velocities induced during deployment. Following this, the spacecraft will enter into its science mode, where the spacecraft will spin on one of its shorter body axes (body x-axis) in orbit.

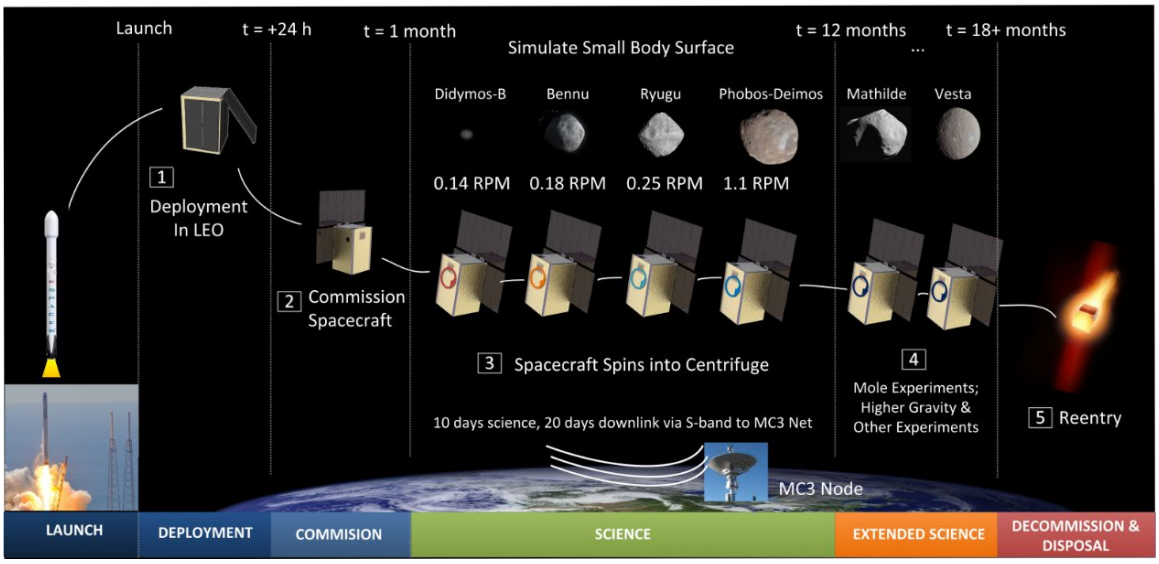

Figure 1. The Concept of Operations of the AOSAT+ mission.

The concept development of AOSAT+ and future CubeSat centrifuge missions is being done through a NASA-supported center called ASTEROID (Asteroid Science, Technology and Exploration Research Organized by Inclusive eDucation (ASTEROID) housed at University of Arizona (UA). This proposed program envisions project-centric, hands-on education that would place UA students and transfer students from the nearby Pima Community College and the University of Puerto Rico, Humacao in cutting-edge research labs at the UA and in direct collaboration with NASA JPL. UA, Pima, and Univ. of Puerto Rico students would be tasked with developing an exciting series of CubeSat missions

By the centrifugal action of the spacecraft, AOSAT+ will be able to simulate the surface gravity of a target body of interest. The requirement of the primary mission objective is that the attitude control system must be able to spin the spacecraft at speeds up to 1.1 RPM. The spacecraft will remain in the science mode for about 10 days spinning at different angular velocities between 0.1 RPM − 1.1 RPM. After the 10 day period, the spacecraft will communicate its data to the Mobile CubeSat Command and Control (MC3) network of ground-stations operation by the Space Dynamics Laboratory [6]. These operations are cycled for about 1 year. These operations will enable AOSAT+ to meet its primary science objectives. After this, the spacecraft will operate in an extended science mode where the spacecraft will be commanded to spin at higher spin rates and active experiments such as impact strength measurement would be performed on the spinning

regolith. While the science returns of the AOSAT+ are quite exciting, there are several interesting engineering challenges that need to be addressed for a successful implementation of the mission. This work will provide an overview of the attitude control system development for AOSAT+ mission concept.

The organization this work is as follows: Section II presents relevant work done in the microgravity simulations for space applications, and related attitude control problems. Section III describes the AOSAT+ spacecraft. Section IV present attitude dynamics and Section V presents preliminary simulation results followed by conclusion.

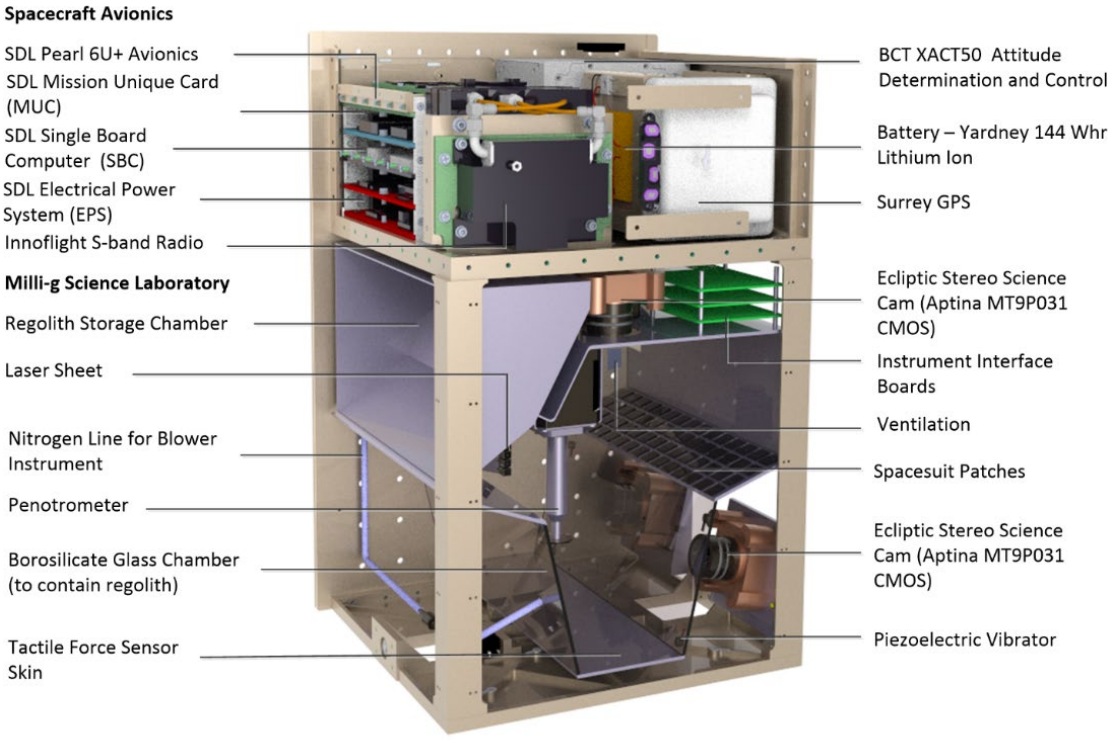

Figure 2: AOSAT+ Internal Layout

RELATED WORK

Simulating asteroid surface conditions remains a formidable challenge. The challenge comes from simulating the low-gravity conditions. Conventional methods of generating low-gravity conditions include parabolic flights [7], neutral buoyancy water tanks [8], and drop towers [9]. These methods simulate the required low gravity conditions either for a brief period, or present artifacts that cannot directly be correlated to that of asteroid surface conditions. A space-based centrifuge, on the other hand, appears to be a promising platform to simulate these low gravity conditions [10]. Space-based centrifuges have tested onboard the International Space Station (ISS) as a platform for several fundamental and biological experiments [11]. While ISS based centrifuges do offer a stable low-gravity platform, the random perturbative accelerations injected by the ISS subsystems [12] are comparable to the smallest target microgravity conditions of our experiments (10^{-5} g). This coupled with the low-cost feasibility and rapid miniaturization of CubeSat technologies [13] suggests that a dedicated orbiting CubeSat centrifuge as an ideal platform for our experiments.

Our first CubeSat centrifuge laboratory mission is called Asteroid Origins Satellite-1 (AOSAT-1) [14, 15]. The spacecraft is a 3U CubeSat, with the science chamber spanning two units (2U) of volume. This design provided an estimated moment arm of 20 cm. The Centrifuge mode of the AOSAT-1 mission requires that the spacecraft be spun at a constant 1 RPM, about its long axis, thus generating a peak centrifugal acceleration of 2.23×10^{-4} g (1 g = $9.81 \frac{\mathrm{m}}{\mathrm{s}^2}$), which is indicative of the gravity of sub a 1 km diameter asteroid [16]. The spacecraft will use a combination of reaction wheels and magnetorquers to achieve this attitude mode [17]. In comparison, the AOSAT+ is a larger spacecraft with a 12U CubeSat form factor [18]. The top 4U portion of the CubeSat spans the spacecraft avionics, while the remaining 8U spans the instruments, spin chamber, and the regolith required for the experiments as shown in Fig. 4. Despite similar moment arm lengths, AOSAT+ will be spun at multiple spin rates when compared to AOSAT-1, thus enabling it to generate the conditions of multiple target bodies as shown in Figure 1.

The attitude dynamics and control of spinning spacecraft is well studied in the literature and several representations to study spacecraft attitude have been developed [23, 24]. The modified Rodriguez parameters (MRPs) [25] are one of the many convenient ways to represent spacecraft attitude as they form a minimal set representation [24] of the spacecraft attitude. Several spin-stabilized spacecraft, where a principal axis spin is used to regulate the attitude of the spacecraft, have been successfully flown [26]. The primary challenge to a spinning spacecraft comes from fluctuations in the net moment of inertia tensor of the spacecraft [27]. Important sources of such fluctuations arise from moving components such as fuel slosh [28, 29], solar panel deployment [30], and solar panel flexing [31]. The fuel sloshing is a phenomenon that occurs when a spacecraft carrying fuel is subjected to large maneuvers. Existing studies model the slosh as an oscillating pendulum and describe the perturbation due to the slosh as a dissipating energy function [32]. The solar panel deployment of a satellite takes place during the initial phase of the mission when its initially stowed solar panels are expanded to increase the Solar power input to the spacecraft. Since AOSAT+, similar to many small spacecraft, has a one-time solar panel deployment mechanism, this will not be a repeating source of perturbations. The solar-panel flexing, on the other hand, is due to the structural vibrations of the solar panels. While this is indeed a major source of perturbation for large spacecraft, the current work does not include the solar panel flexing because of the small spacecraft form factor of the spacecraft. It should be noted here that while the inertia fluctuations due to moving regolith are similar to the fluctuations arising from fuel slosh, the key difference lies in the fact that slosh results from the fluidic motion of the fuel, while the regolith motion is primarily dominated by the particle dynamics, and their collisions.

SPACECRAFT AND MISSION OPERATIONS

This section presents a detailed overview of the AOSAT+ spacecraft and its mission operations. We begin with a description of the spacecraft subsystems followed by the different mission modes of the spacecraft. These modes correspond to the different attitude maneuvers required by the AOSAT+ Mission Concept.

Avionics

As mentioned in the previous section, the AOSAT+ spacecraft is a 12U CubeSat which has a total estimated mass of 24 kg, of which the regolith carried is about 3 kg. Fig. 2 shows a computer-aided design (CAD) representation of the AOSAT+ spacecraft assembly. The 12U bus will be developed by the Space Dynamics Laboratory (SDL). The design provides an estimated mass margin of 25% and volume margins of 44% [5]. The spacecraft uses an SDL built Single Board Computer containing Cobham Leon 3FT rad-hardened processor operating at 125 MHz coupled with a rad-tolerant Micro-semi FPGA, 256 Mb of SDRAM and 16 GB solid-state drive. The SBC board

interfaces to the Mission Unique Card (MUC) via SpaceWire. The MUC hosts all the science instruments. The spacecraft will use the Innoflight SCR-101 S-band Radio capable of 1.5 Mbps data rate. The system is designed to send/receive at least 8bit tone data with a 6 dB margin even if the spacecraft is spinning. The SDL will be providing spacecraft tracking and communication services using the MC3 communications network.

Attitude Determination and Control System

The AOSAT+ uses the XACT 50 module from Blue Canyon Technologies to monitor and control its attitude. The architecture of the ADCS unit of AOSAT+ is presented in Fig. 3. This subsection presents the capabilities of the XACT 50 module.

Attitude Determination System. The attitude determination system (ADS) of the XACT 50 unit uses a star tracker; an IMU which comprises of a MEMS gyroscope, a magnetometer, and an accelerometer; and a Sun sensor. The XACT 50 unit runs a pre-programmed Kalman filter [33] attitude estimation algorithm with an estimated $1-\sigma$ pointing accuracies in the range of $0.003-0.007$ deg on all 3 axes. It is pointed out here that the accuracy of the attitude determination is expected to decrease during the centrifuge mode, especially while centrifuging at the maximum target rotation rates. However, during this mode spacecraft pointing will not be of concern, since the spacecraft will be sufficiently charged and prior to entering.

Attitude Control System. The attitude control system (ACS) of the XACT 50 unit uses reaction wheels and magnetorquers on all 3 axes. The XACT 50 unit uses a set of three RWp050 reaction wheels placed along 3 mutually perpendicular axes. Each reaction wheel has an estimated mass of 0.24 kg and a diameter of 5.8 cm.

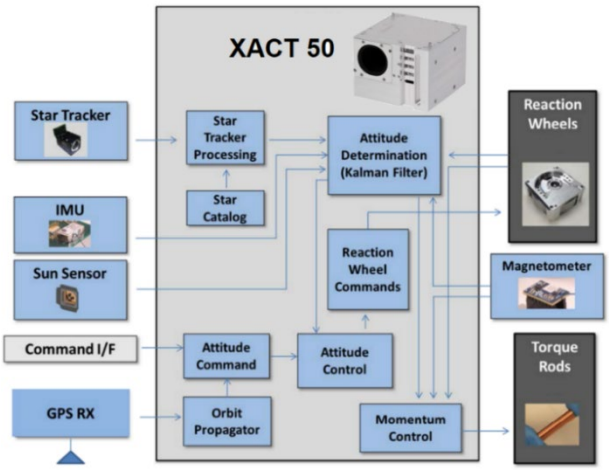

Figure 3. The hardware architecture of the XACT 50 module, the selected ADCS unit of AOSAT+.

The reaction wheels can spin at a maximum speed of about 4731 RPM, to account for maximum angular momentum storage of 0.05 Nms. The reaction wheels can produce a maximum control torque of 0.007 Nm. The magnetorquers of the XACT 50 module have a maximum control dipole of 0.2 Am^2. The ADCS unit will be provided with preprogrammed operations such as spacecraft detumbling, pointing, and reaction wheel desaturation.

Milli-g Science Laboratory Chamber

The payload containing the spin chamber, and the sensor suite will be referred to as the milli − g science lab chamber. As seen in Fig. 2, the lab chamber spans the lower 8U volume of the to maximize the moment arm of the spacecraft spin. The regolith will initially be stored in the regolith storage chamber which is from the borosilicate glass chamber by a door mechanism. The door will be controlled by a burn-wire release mechanism. Upon triggering this during the start of the first science mode, the door drops, and the regolith comes out into the glass chamber aided by centrifugal. The glass chamber contains spacesuit material coupons, tactile force sensors, optical cameras. The force sensors will be placed at the bottom end of the lab chamber as shown in Fig. 2, where the maximum moment-arm inside the lab chamber can be experienced during the Centrifuge mode. Additionally, two stereo camera pairs consisting of four Aptina MT9P031 CMOS cameras will image and record the regolith during the experiments [5].

Regolith. A pool of asteroid regolith is flown inside the spacecraft which is produced by fragmenting 2.5 kg of a meteorite into a size distribution from 1 mm to 10 mm. We use the carbonaceous chondrite Allende, whose parent body may have been compositionally similar to our science targets, with which we have worked extensively. Numerical simulations of regolith dynamics indicate that the pool will be spanned by 9×10^4 - 1×10^5 regolith particles [34].

Power System

The spacecraft will be powered using two large body-mounted deployable MMA eHawk solar panels containing triple-junction cells. The eHawk configuration will avoid gimbaling in order to simplify the spacecraft operation. The system will charge a bank of 144 Whr Yardney Lithium-Ion batteries. The depth of discharge will not exceed 20 % to maximize battery capacity and life. Preliminary power budget analysis suggests a 25 % power margin [5].

Spacecraft Configurations and Reference Frame

As a result of solar panel deployment, the AOSAT+ spacecraft will essentially operate in two structural configurations. The first configuration will have stowed solar panels. After the initial detumbling, the spacecraft will deploy its solar panels and enter its second configuration. This deployment will cause the spacecraft to change its dynamic parameters such as the center of gravity, and the moment of inertia. Consequently, the motion of the spacecraft will be expressed in different reference frames. The spacecraft motion of interest to the current work is its attitude dynamics. The two configurations and their corresponding reference frames are depicted in Fig. 4. The reference frames used to describe the spacecraft attitude in both these cases are defined as follows:

Origin. The origins of the body frames in both configurations are located at their corresponding center of mass.

z-axis. The z-axis of both configurations will point downwards along the length of the spacecraft.

x-axis. In the stowed configuration, the x-axis will point along a direction parallel to the plane of the solar panels after their deployment. Once the panels are deployed, the stowed configuration reference frame will be rotated by a 90 deg counterclockwise rotation along its z-axis, which results in an x-axis which points normally outward from the plane of the deployed solar panels as shown in Fig. 4.

y-axis. The completes is defined using the right-hand rule over the x and z axes.

The left superscripts B_S, and B_D the body frame in the stowed and deployed configurations respectively. The frames are so defined in order to arrange the body frame principal moments of inertia along the $x, y,$ and z axes—J_x, J_y, and J_z-- will be sorted in the descending order convention, i.e., $J_x \geq J_y \geq J_z$, in both the coordinate frames [24]. In addition, the regolith motion also causes a change in the moment of inertia as described in Section IV. The regolith deployment occurs after the solar panels are deployed and before the spacecraft is ready to enter its first centrifuge operation. For this reason, in the deployed configuration, we note two types of inertia tensors. The first is when the solar panels are deployed, and the regolith is tightly stowed inside the storage chamber. The second parameter is the inertia only arising due to the stationary parts of the spacecraft, which corresponds to all subsystems except the regolith particles. This parameter is useful for modeling the centrifuge of the spacecraft, where the inertia due to the regolith is superimposed using a three-dimensional parallel axis theorem [24].

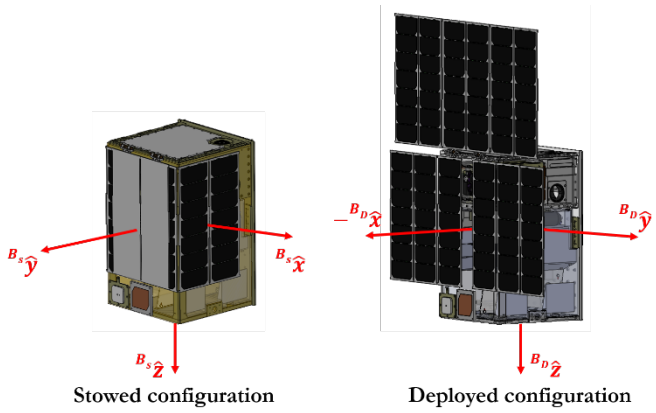

Figure 4. The two structural configurations of AOSAT+, and their corresponding body frames. The origin of both frames is located at their corresponding center of mass.

Additionally, the CAD model indicates that the maximum moment arm from the spacecraft center of mass to the center of the chamber edge will be about 23 cm when no regolith is present inside the spacecraft. The structural parameters of the AOSAT+ spacecraft in the deployed configuration are summarized in Table 1.

Baseline Orbit Parameters

A low-Earth orbit was selected for AOSAT+ such that the access to the MC3 ground-station network was sufficient to meet the link margin requirements of the mission concept. The orbital elements of the selected AOSAT+ orbit are listed in Table 2. The baseline orbit is used to define an instantaneous spacecraft reference frame, depicted in Fig. 5, in order to define the attitude. The origin and the basis vectors of the spacecraft presented are defined as follows:

Table 1. Dynamical parameters of the spacecraft in the deployed configuration.

Parameter	Value
Fixed spacecraft mass m_w, (kg)	20

Mass of regolith m_r, (kg)	2.5
Nominal max. moment arm length, r_c (cm)	23.0
Moment of inertia due to the fixed mass J_{ch}, (kg m^2)	$\begin{bmatrix} 0.343 & 0 & 0 \\ 0 & 0.224 & 0.01 \\ 0 & 0.01 & 0.326 \end{bmatrix}$

Origin. The origin of the orbit frame coincides with the spacecraft center of mass.

y-axis. The y-axis points along the direction of the spacecraft velocity with respect to the Earth-centered inertial J2000 reference frame N [35].

z-axis. The z-axis points towards the center of the Earth.

x-axis. The x-axis is defined by using the right-hand rule over the y and z axes.

A left superscript O beside a vector is used to indicate that the vector is resolved in the Orbital frame. The attitude maneuvers, of interest, in the current work, will be the orientation of the spacecraft body frames relative to the orbit reference frame.

Table 2. Orbital elements of the selected orbit for the AOSAT+ spacecraft.

Orbital Element	Value
Semi-major axis	6,928 km
Eccentricity	0
Inclination	43 deg
RAAN	90 deg
Argument of periapsis	0 deg

Mission Modes

After its deployment in the baseline orbit, the AOSAT+ spacecraft will start executing its mission operations. The operations are categorized into a set of spacecraft attitude modes. From an attitude control design perspective, the AOSAT+ spacecraft will have six modes of operation: Detumble, Panel deployment, Regolith deployment, Reference tracking, Desaturation modes, and Centrifuge modes.

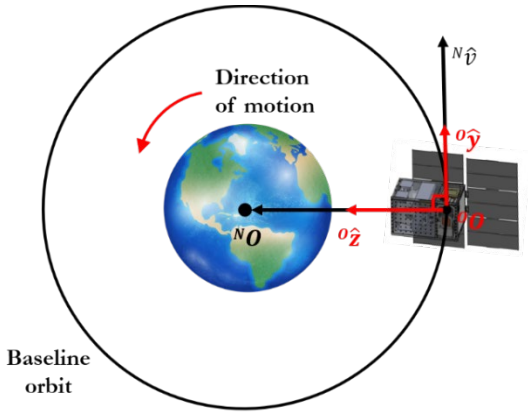

Figure 5. The selected orbital frame of the spacecraft depicted in its orbital frame. The *x*-axis (not shown here) completes the right-hand triad and is along the outward normal direction to the orbital plane.

Detumble Mode. The Detumble mode occurs during the commissioning phase of the mission. The objective of this operation is to nullify any angular velocities on the spacecraft induced during deployment from the CubeSat dispenser. In this mode, the regolith is secured tightly in its storage chamber and the solar panels are in the stowed configuration. The spacecraft will use only the magnetorquers to regulate its angular velocity vector. At the end of this maneuver, the spacecraft will be able to begin its attitude acquisition.

Panel Deployment Mode. Once the spacecraft finishes its attitude acquisition, The AOSAT+ spacecraft will deploy its solar panels. During this operation, the spacecraft changes between its two structural configurations shown in Fig. 4. The attitude control system will ensure that this deployment does not cause the spacecraft to tumble.

Regolith Deployment Mode. Before beginning its experiments, the regolith stored inside the storage chamber will be allowed to enter into the science lab chamber. As mentioned above, the entry of the regolith into the chamber is blocked by a trapdoor which is secured by a burn wire mechanism. Upon a trigger, the locking wire is burnt, and the regolith now flows into the laboratory. This passage causes the inertia of the spacecraft to fluctuate. Similar to the Panel deployment mode, the attitude control system ensures that the spacecraft does not tumble during the regolith deployment.

Tracking Mode. A typical space mission requires its spacecraft to track a certain reference trajectory. This could be a rest-to-rest maneuver such as reorienting the spacecraft after a detumbling operation or enabling the appropriate subsystems to track time-varying vectors such as the ground station or the Sun. It is pointed here that since the AOSAT+ configuration varies with the deployment of solar panels and the regolith; each configuration will use a separate Tracking mode.

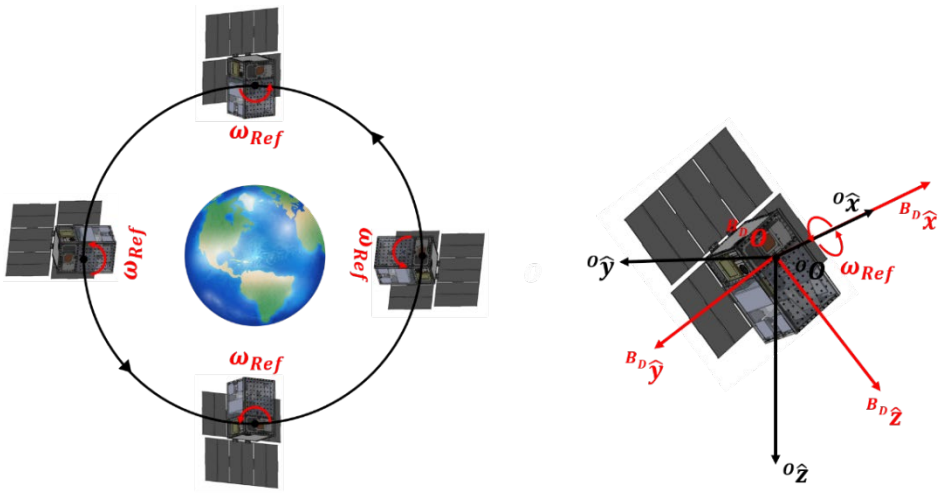

Figure 6. Illustration of the Centrifuge mode if AOSAT+ showing the orbital motion of the spacecraft (left) and attitude motion profile (right).

Desaturation Mode. The Desaturation mode is responsible for dissipating the angular momentum built up in the reaction wheels over a long period of time due to the disturbance torques acting on the spacecraft. In this mode, the spacecraft uses its magnetorquers to dissipate the angular momentum of the wheels.

The five modes described here are a general characteristic of most spacecraft missions as they primarily require that the spacecraft does not tumble, or that the spacecraft be oriented along a particular direction with respect to the orbital frame. As a result, the controllers for these operations will be available as pre-programmed operations into the ADCS unit. The science mode, on the other hand, is a mission-specific operation, which requires a custom-developed controller.

Centrifuge Mode

The centrifuge operation forms the core of all the experiments planned by AOSAT+. In this mode, the spacecraft will be commanded to enter a counterclockwise spin of magnitude ω_{Ref} about the orbit frame x-axis as illustrated in Fig. 6. The rotations will produce a radially outward centrifugal acceleration on the regolith particles whose magnitude is given by

$$a_c = r_c \omega_{Ref}^2 \tag{1}$$

For a selected spin rate ω_{Ref}, the centrifugal acceleration will increase with increasing radial length, as observed from Equation 1, and inside the lab chamber of the AOSAT+ spacecraft, this will be maximum at the bottom end of the glass chamber where the tactile force sensors will be placed. The objective of the Centrifuge mode is to subject the regolith particles at the bottom end of the lab chamber to a centrifugal acceleration corresponding to a selected small body gravity regime by spinning at a target angular velocity. Thus, by selecting an appropriate spin rate ω_{Ref}, a centrifugal acceleration which is equivalent to an asteroid surface gravity level can be imparted onto the regolith particles at the end of the glass chamber. During its science phase, the spacecraft

will aim to simulate the gravity regimes of four different small bodies in the Solar system [5] at the end of its glass chamber, by spinning at four different spin-rates as shown in Fig. 6. The different spin rates and target bodies are summarized in Table 3. The radial moment arm used in the computation of the centrifugal acceleration is noted from Table 1.

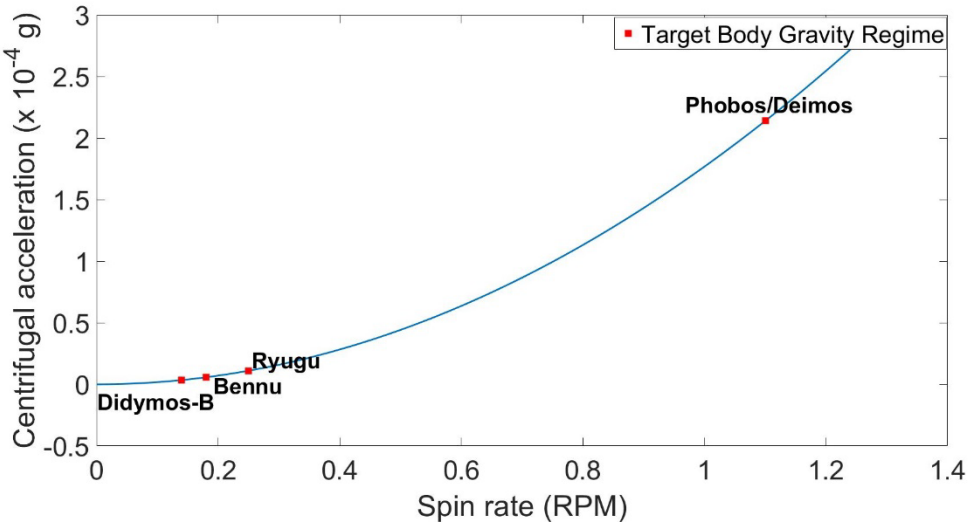

Figure 7. The small body gravity regimes targeted by the Centrifuge mode of AOSAT+, along with the required spacecraft spin magnitude.

It should be noted here that the particles inside the chamber will be affected by other accelerations and perturbations, and that the centrifugal acceleration experienced by the regolith particles will vary based on its radial distance to the center of gravity. However, the insights from these experiments are still sufficient to meet the science objectives of AOSAT+ [5].

ATTITUDE DYNAMICS

The primary interest here is the attitude of the spacecraft body frame with respect to its orbital frame. Let the attitude spacecraft body frame with respect to its orbit frame be denoted by the Modified Rodriguez Parameters (MRPs) $\bar{\boldsymbol{\sigma}}$ [25], with its vector components given by σ_x, σ_y, and σ_z, and magnitude is given by σ. Let $\bar{\omega}$ denote the angular velocity of the spacecraft body frame with respect to its orbit frame, and $\bar{\Omega}$ denote a 3×1 vector containing the angular velocities of the three reaction wheels onboard the spacecraft. The time evolution of the MRPs is governed by the following kinematic differential equation [20].

$$\dot{\bar{\boldsymbol{\sigma}}} = \frac{1}{4}[B(\bar{\boldsymbol{\sigma}})]\bar{\omega} \tag{2}$$

where the matrix function $[B(\bar{\boldsymbol{\sigma}})]$ is defined as

$$[B(\bar{\boldsymbol{\sigma}})] = (1 - \sigma^2)[I] + 2[\tilde{\boldsymbol{\sigma}}] + 2\bar{\boldsymbol{\sigma}}\bar{\boldsymbol{\sigma}}^{\boldsymbol{T}} \tag{3}$$

where $[I]$ is the 3×3 identity matrix. The evolution of MRP's periodically capped by switching to a shadow set in order to prevent controller unwinding using the relation

$$\bar{\boldsymbol{\sigma}} = -\frac{\bar{\boldsymbol{\sigma}}}{\sigma^2} \quad \text{if } \sigma > 1 \tag{4}$$

In order to derive the attitude dynamics which accounts for the inertia fluctuation, consider the spacecraft angular momentum [20] $\bar{H}$ given by

$$\bar{H} = [J]\bar{\omega} + [W_s]\bar{h}_s \tag{5}$$

Where, $[W_s]$ is the wheel alignment matrix whose columns denote the spin axes of the reaction wheels with respect to the spacecraft body frame, and $\bar{h}_s$ denotes the reaction wheel angular momentum, whose cartesian components are given by:

$$h_{s_i} = J_{s_i}(\Omega_i + \bar{\omega}.\hat{w}_{s_i}) \tag{6}$$

Where J_{s_i} is the moment of inertia of the reaction wheel along the i^{th} direction, and $\hat{w}_{s_i}$ is the i^{th} column of $[W_s]$. Differentiating Equation 5 using the transport theorem gives

$$\begin{aligned} \dot{\bar{H}} &= \bar{\tau}_{ext} \\ &= [J]\dot{\bar{\omega}} + [\dot{J}]\bar{\omega} + [\tilde{\bar{\omega}}]([J]\bar{\omega} + [W_s]\bar{h}_s) - [W_s]\bar{U}_C \end{aligned} \tag{7}$$

Where $\bar{\tau}_{ext}$ denotes the vector sum of any disturbance torques acting on the spacecraft, and $\bar{U}_{RW}$ is the reaction wheel control torque whose components are given by

$$U_i = -J_{s_i}(\dot{\Omega}_i + \dot{\bar{\omega}}.\hat{w}_{s_i}) \tag{8}$$

Additionally, Equation 8 can be solved for $\dot{\Omega}_i$ in order to describe the time evolution of the reaction wheel angular velocities. Equation 7 can now be rewritten to describe the evolution of the spacecraft angular velocities as

$$\begin{aligned} \dot{\bar{\omega}} = &-[J]^{-1}([\tilde{\bar{\omega}}]([J]\bar{\omega} + [W_s]\bar{h}_s)) - [J]^{-1}[\dot{J}]\bar{\omega} \\ &+ [J]^{-1}\bar{\tau}_{ext} + [J]^{-1}[W_s]\bar{U}_{RW} \end{aligned} \tag{9}$$

It is noted here that Equation 9 is largely similar to the standard Euler's equation of attitude dynamics [20]. However, the standard form is now modified to also describe the effect of regolith fluctuations of the spacecraft attitude through the $[J]^{-1}[\dot{J}]\bar{\omega}$ term.

SIMULATION AND RESULTS

The results of the Centrifuge mode simulations for different test cases are presented here. We begin by noting the peak disturbances, spacecraft attitudes, and centrifugal accelerations generated at the bottom of the simulated laboratory chamber are noted here.

Case $N = 100$: The spacecraft was initialized with 10 random initial conditions per reference spin rate magnitude as described above. The attitude of the spacecraft was controlled using the sliding mode controller with gains in Table 3. The effect of regolith fluctuation torque ($[J]^{-1}[\dot{J}]\bar{\omega}$), along with the other disturbance torques modeled in the current work, are presented in the semi-log plot in Figure 8. As seen here, the inertia fluctuation presents the dominant source of disturbance

torques, on the order of 10^{-4} N − m in the first two studies which have lower target spin rate magnitudes. The maximum inertia fluctuation torque occurred around of 10^{-3} N − m when the target spin rate was a maximum of 1.1 RPM. The inertia fluctuation torques are followed by the gravity gradient (around $10^{-8} - 10^{-7}$ N − m), SRP (around 10^{-7} N − m), and the drag torques (around 10^{-10} N − m).

Table 3. The selected gain parameters used in implementing the sliding mode control law.

Parameter	Value
K_P (rad/s)	$0.14\, I$
K_I (rad/s^2)	$5.4 \times 10^{-4} I$
η (rad/s^2)	$[0.01 \quad 0.5 \quad 0.5]^T$
Φ (rad/s)	$[1 \quad 1 \quad 1]^T$
$\bar{\tau}_{max}$ (N − m)	$10^{-5}[1 \quad 1 \quad 1]^T$

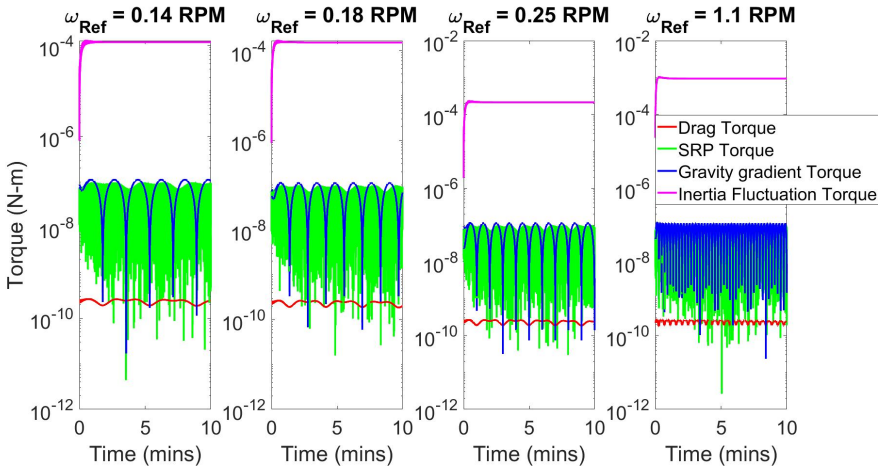

Figure 8. Disturbance torques acting on the simulated Centrifuge mode at different target spin rates, when the chamber has $N = 100$ particles.

The response of the spacecraft angular velocity components, and the MRP components are presented in Figures 9 and 10 respectively. As seen in Fig 18, the simulations indicate that the spacecraft is able to steadily achieve the desired spin rates within 1.5 mins. Figure 10 suggests that the spacecraft is able to track its reference MRP, which indicates that the spin axis is kept aligned with the orbital x-axis.

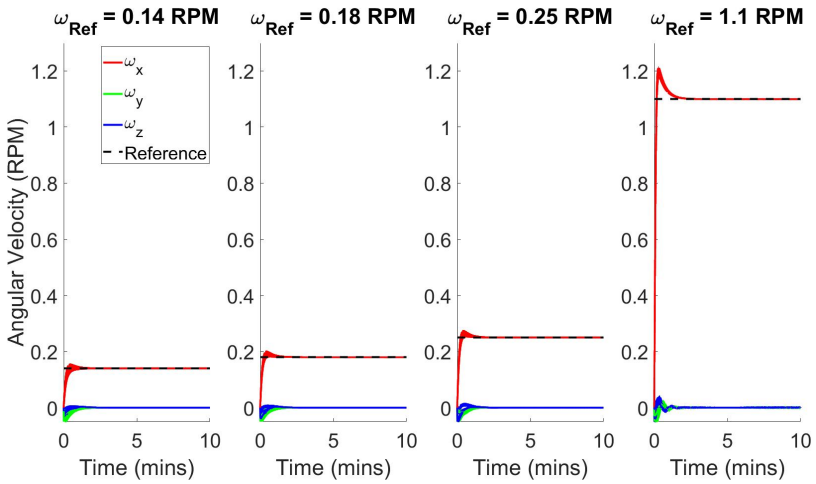

Figure 9. Spacecraft angular velocity response for different target spin rates of the Centrifuge mode, when the chamber has $N = 100$ particles.

The centrifugal accelerations generated at the bottom of the AOSAT+ laboratory chamber are presented in Figure 11. As seen here, the magnitude of centrifugal acceleration at the bottom of the laboratory chamber is able to meet the gravity levels of their target small bodies.

Case $N = 1000$: The disturbance torques modeled on the spacecraft are presented in Figure 12. As seen here, the inertia fluctuation torque is largely on the same order of magnitude (around 10^{-7} N − m) as the gravity gradient and the SRP torques at slower rotation speeds. The magnitude is seen to steadily go up to 10^{-6} N − m at the maximum target spin rate of 1.1 RPM.

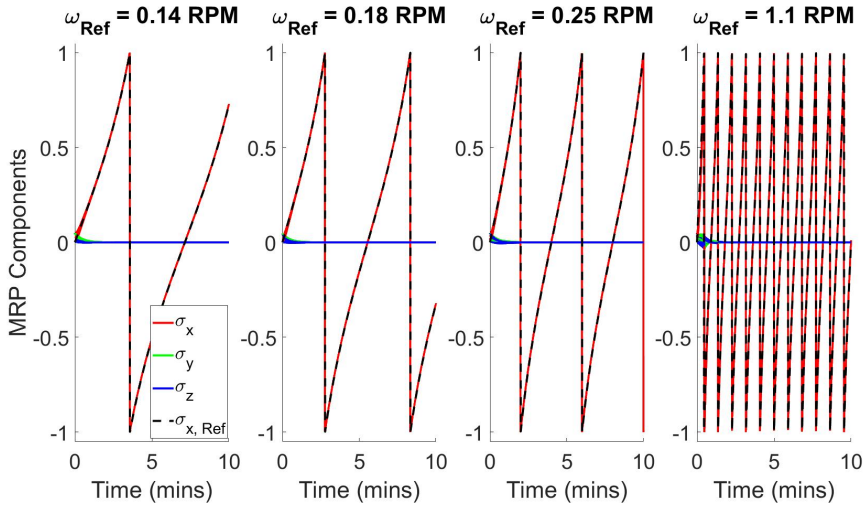

Figure 10. Time response of the spacecraft MRP components at different target spin rates of the Centrifuge mode, when $N = 100$ particles.

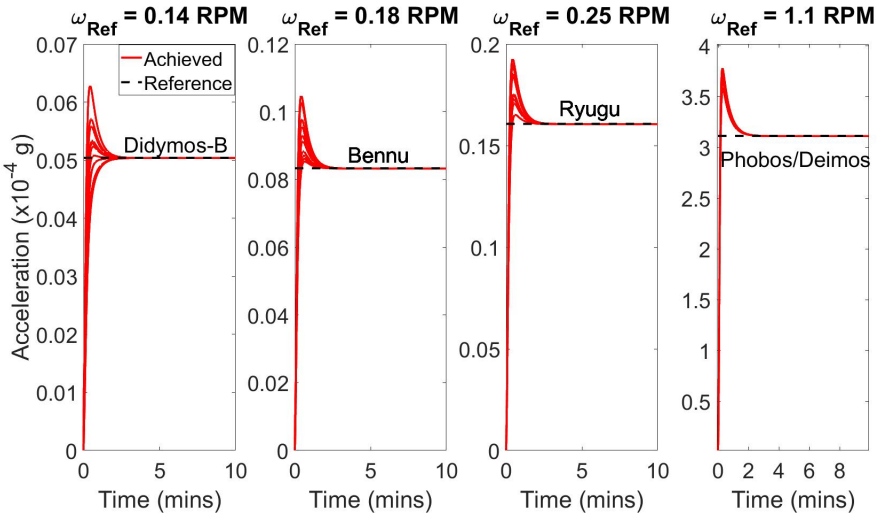

Figure 11. Magnitude of centrifugal accelerations generated at the bottom of the AOSAT+ laboratory chamber when $N = 100$ particles.

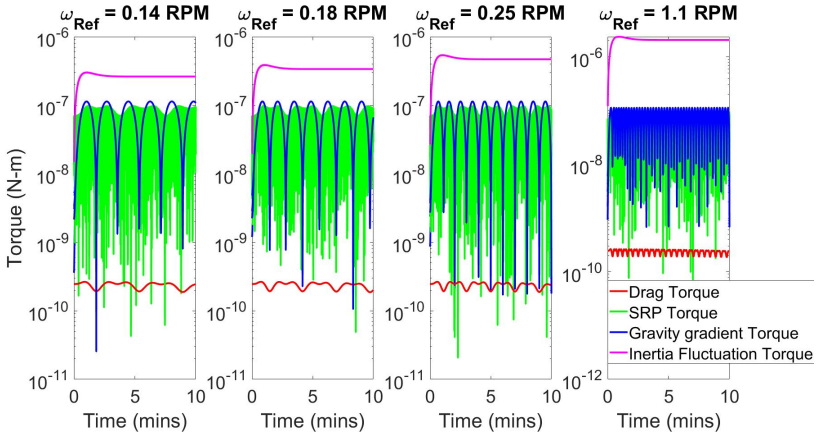

Figure 12. Disturbance torques acting on the simulated Centrifuge mode at different target spin rates, when the chamber has $N = 1000$ particles.

The response of the spacecraft angular velocity components is presented in Figure 13. As seen here the spacecraft is able to track the desired target spin rates about the orbital x-axis within 3 minutes. The time evolution of the MRP components of the spacecraft (not shown here) is noted to follow the same reference trajectory noted in Figure 10.

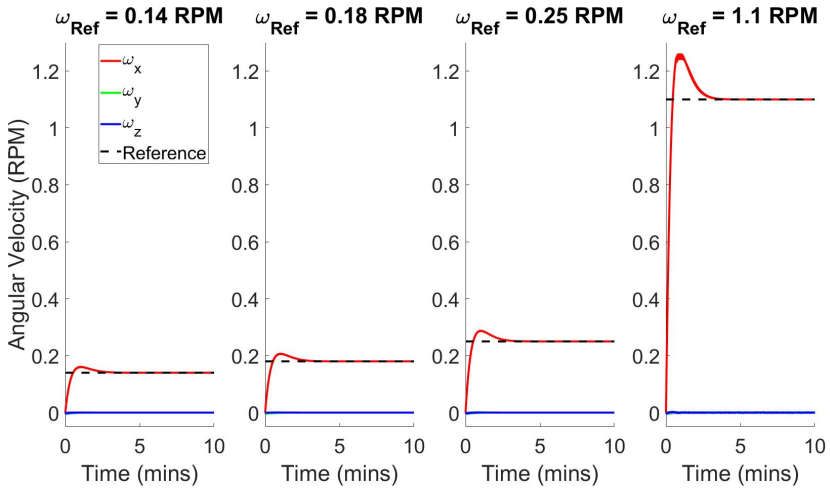

Figure 13. Spacecraft angular velocity response for different target spin rates of the Centrifuge mode, when the chamber has $N = 1000$ particles.

The centrifugal accelerations generated at the bottom of the AOSAT+ laboratory chamber, are presented in Figure 14. As seen here, the magnitude of centrifugal acceleration at the bottom of the laboratory chamber is able to achieve the gravity levels of their target small bodies.

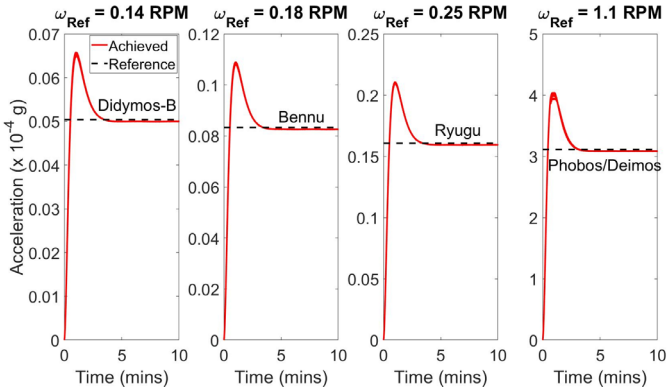

Figure 14. Centrifugal accelerations generated at the bottom of the AOSAT+ laboratory chamber when $N = 1000$ particles.

The results of the simulation in the current work provide key insights into implementing the Centrifuge mode of AOSAT+. Firstly, for a constant net regolith mass, the disturbance torques decreased as the number of regolith particles in the simulated pool increased. As a baseline estimate, the disturbance torques arising from fluctuating regolith is noted to be around $10^{-6} - 10^{-7}$ mN − m, and can become the dominant source of perturbation torques at high-speed target rotations of around 0.25 to 1.1 RPM. Secondly, the designed sliding mode control torque is capable of rotating the spacecraft at all its target rotation speeds in the presence of inertia fluctuations, parametric uncertainties, and orbital disturbances. Additionally, the control torques generated during the simulations were well within the boundaries of the selected BCT XACT-50 attitude determination and control system (ADCS) module, where simulations indicate that the spacecraft can converge to its target speeds within 3 mins by using about 36 % of the peak actuator torque.

Finally, the simulations and an angular momentum exchange analysis suggest that the RWp050 reaction wheels of the XACT-50 module are capable of meeting all the requirements of the Centrifuge mode is the nominal case, where regolith is assumed to be evenly distributed about the center of the laboratory chamber. However, the current work also identifies that some worst-case distributions can saturate the reaction wheels when trying to spin the spacecraft its maximum target spin rate of 1.1 RPM. However, this allows us to better design the laboratory chamber of the spacecraft, in order to make ensure the successful operation of the AOSAT+ spacecraft.

CONCLUSIONS

This work presented the goals and challenges of the AOSAT+ Mission Concept from an attitude control perspective. The AOSAT+ is a 12U CubeSat whose objective is to simulate the gravity of small bodies such as asteroids, by acting as a dedicated space-based centrifuge for 2.5 kg of crushed Allende meteor regolith. During this centrifuging maneuver, the spacecraft will be spun at different target spin rates about its body axis, which will then induce centrifugal acceleration components that correspond to gravity levels of a target asteroid at the maximum radial moment arm. We began by presenting a detailed description of the AOSAT+ spacecraft, and its subsystems. The different planned modes of spacecraft operation were also presented. While most of these planned operations are typical of any spacecraft mission with three axis-attitude control, the Centrifuge mode of AOSAT+ mission is a unique mission operation as it requires the spacecraft to be spinning about a fixed axis during its orbit. Additionally, the Centrifuge mode will also contain moving regolith particles which will cause the moment of inertia to fluctuate during the mission. In order to address this, we derived a robust control law that can handle the inertia fluctuations and other parametric uncertainties. The control law was successfully demonstrated in simulation at all the target spin rates for the nominal spacecraft design. These results raise confidence in development of a larger, 12U CubeSat for use as on-orbit centrifuge laboratory.

REFERENCES

[1] D.S. Lauretta, S.S. Balram-Knutson, E. Beshore, W. Boynton, C.D. d'Aubigny, D.N. DellaGiustina, H.L. Enos, D.R. Golish, C.W. Hergenrother, E.S. Howell and CA Bennett, 2017. OSIRIS-REx: sample return from asteroid (101955) Bennu. *Space Science Reviews*, *212*(1-2), pp.925-984.

[2] Y. Tsuda, M. Yoshikawa, M. Abe, H. Minamino. and S. Nakazawa, S., 2013. System design of the Hayabusa 2—Asteroid sample return mission to 1999 JU3. *Acta Astronautica*, *91*, pp.356-362.

[3] P.E. Michel et al., 2015. *Asteroids IV*, University of Arizona Press.

[4] J.C. Castillo-Rogez, M. Pavone, J.A. Hoffman, and I.A. Nesnas, 2012, March. Expected science return of spatially extended in-situ exploration at small solar system bodies. In *2012 IEEE Aerospace Conference* (pp. 1-15). IEEE.

[5] Thangavelautham, J., Asphaug, E. and Schwartz, S., 2019, March. An On-Orbit CubeSat Centrifuge for Asteroid Science and Exploration. In *2019 IEEE Aerospace Conference*. IEEE

[6] R.C. Griffith, 2011. *Mobile CubeSat command and control (MC3)*. Naval Postgraduate School, Monterey Ca.

[7] L.M. Sharp, 2011. *Three-dimensional critical wetting experiment in commercial zero-gravity space flight* (Doctoral dissertation, Purdue University).

[8] J.C. Jairala, R. Durkin, R.J. Marak, S.A. Sipila, Z.A. Ney, S.E. Parazynski, and A.H. Thomason, 2012. EVA Development and Verification Testing at NASA's Neutral Buoyancy Laboratory.

[9] W.A. Dittrich, 2014. Drop Tower Physics. *The Physics Teacher*, *52*(7), pp.415-417.

[10] L.R. Young, 2011, March. Spinning our way to Mars. In *Proceedings of the 2011 IEEE Aerospace Conference* (pp. 1-2). IEEE Computer Society.

[11] A.L. Paul and R.J. Ferl, 2015. Spaceflight exploration in plant gravitational biology. In *Plant Gravitropism* (pp. 285-305). Humana Press, New York, NY.

[12] G.H. Kitmacher, 2006. *Reference guide to the international space station*.

[13] Nason, I., Puig-Suari, J. and Twiggs, R., 2002, March. Development of a family of picosatellite deployers based on the CubeSat standard. In *Proceedings, IEEE Aerospace Conference* (Vol. 1, pp. 1-1). IEEE.

[14] J. Lightholder, A. Thoesen, E. Adamson, J. Jakubowski, R. Nallapu, S. Smallwood, L. Raura, A. Klesh, E. Asphaug, and J. Thangavelautham, 2017. Asteroid origins satellite (AOSAT) I: an on-orbit centrifuge science laboratory. *Acta Astronautica*, *133*, pp.81-94.

[15] Asphaug, E. and Thangavelautham, J., 2014, March. Asteroid regolith mechanics and primary accretion experiments in a CubeSat. In *45th Lunar and Planetary Science Conference* (p. 2306).

[16] Asphaug, E., Thangavelautham, J., Klesh, A., Chandra, A., Nallapu, R., Raura, L., Herreras-Martinez, M. and Schwartz, S., 2017. A CubeSat centrifuge for long duration milligravity research. *npj Microgravity*, *3*(1), pp.1-5.

[17] R. Nallapu, S. Shah, E. Asphaug, J. Thangavelautham*, Attitude control of the Asteroid Origins Satellite 1 (AOSAT 1).* AAS GNC Conference 2017.

[18] Schwartz, S.R., Michel, P. and Richardson, D.C., 2013. Numerically simulating impact disruptions of cohesive glass bead agglomerates using the soft-sphere discrete element method. *Icarus*, *226*(1), pp.67-76.

[19] Richardson, D.C., Quinn, T., Stadel, J. and Lake, G., 2000. Direct large-scale N-body simulations of planetesimal dynamics. *Icarus*, *143*(1), pp.45-59.

[20] Baraff, D., 1997. An introduction to physically based modeling: rigid body simulation II—nonpenetration constraints. *SIGGRAPH course notes*, pp. D31-D68.

[21] Murdoch, N., Sánchez, P., Schwartz, S.R. and Miyamoto, H., 2015. Asteroid Surface Geophysics. *Asteroids IV*, pp.767-792.

[22] Durda, D.D., Movshovitz, N., Richardson, D.C., Asphaug, E., Morgan, A., Rawlings, A.R. and Vest, C., 2011. Experimental determination of the coefficient of restitution for meter-scale granite spheres. *Icarus*, *211*(1), pp.849-855.

[23] F.L. Markley and J.L. Crassidis, 2014. *Fundamentals of spacecraft attitude determination and control* (Vol. 33). New York: Springer.

[24] J. Schaub, J. Junkins, 2014. *Analytical mechanics of space systems* 3rd ed., Reston, Va.: American Institute of Aeronautics and Astronautics.

[25] Terzakis, G., Lourakis, M. and Ait-Boudaoud, D., 2018. Modified Rodrigues Parameters: an efficient representation of orientation in 3D vision and graphics. *Journal of Mathematical Imaging and Vision*, *60*(3), pp.422-442.

[26] Roberson, R.E., 1979. Two decades of spacecraft attitude control. *Journal of Guidance and Control*, *2*(1), pp.3-8.

[27] Janssens, F.L. and van der Ha, J.C., 2011. On the stability of spinning satellites. *Acta Astronautica*, *68*(7-8), pp.778-789.

[28] Ibrahim, R.A., 2005. *Liquid sloshing dynamics: theory and applications*. Cambridge University Press.

[29] Souza, A.G., 2013. Study of the effects of liquid movement and flexibility in performance and robustness of the attitude control system of an artificial satellite [Master of Space Mechanics and Control]. *National Institute for Space Research (INPE), Sao José dos Campos, Brazil*.

[30] Zhengfeng, B. and Yang, Z., 2012. Attitude motion of spacecraft during oblique solar panel deployment. *Aircraft Engineering and Aerospace Technology*, *84*(2), pp.109-114.

[31] DeSouza, L.G., 1970. Robust controller design for a flexible space system using a combination of LQG/LTR and PRLQG methods. *WIT Transactions on The Built Environment*, *22*.

[32] DeSouza, L.G. and de Souza, A.G., 2014. Satellite attitude control system design considering the fuel slosh dynamics. *Shock and Vibration*, *2014*.

[33] E.J. Lefferts, F.L. Markley, and M.D. Shuster, 1982. Kalman filtering for spacecraft attitude estimation. Journal of Guidance, Control, and Dynamics, 5(5), pp.417-429.

[34] Schwartz, S.R., Thangavelautham, J., Asphaug, E., Chandra, A. and Vance, L., 2019. Investigating Asteroid Surface Geophysics with an Ultra-Low-Gravity Centrifuge in Low-Earth Orbit. Proceedings of the 70th International Astronautical Congress, IAF, Washington D.C.

[35] Vallado, D.A, 2013. Fundamentals of Astrodynamics and Applications, Fourth Edition, Space Technology Library.